THE JOURNAL OF PHYSICAL CHEMISTRY Letters

Letter

pubs.acs.org/JPCL

Surface Photovoltage Spectroscopy Study of Organo-Lead Perovskite Solar Cells

Lee Barnea-Nehoshtan, Saar Kirmayer, Eran Edri, Gary Hodes,* and David Cahen*

Department of Materials and Interfaces, Faculty of Chemistry, Weizmann Institute of Science, 76100 Rehovot, Israel

Supporting Information

ABSTRACT: The field of organo-lead perovskite absorbers for solar cells is developing rapidly, with open-circuit voltage of reported devices already approaching the maximal theoretical voltage. Obtaining such high voltages on spun-cast or evaporated thin films is intriguing and calls for detailed investigation of the source of photovoltage in those devices. We present here a study of the roles of the selective contacts to methylammonium lead iodide chloride ($MAPbI_{3-x}Cl_x$) using surface photovoltage spectroscopy. By depositing and characterizing each layer at a time, we show that the electron-extracting interface is more than twice as effective as the hole-extracting interface in generating photovoltage, for several combinations of electrode materials. We further observe the existence of an electron-injection related spectral feature at 1.1 eV, which might bear significance for the cell's operation. Our results illustrate the usefulness of SPV spectroscopy in highlighting gaps in cells efficiency and for deepening the understanding of charge injection processes in perovskite-based photovoltaics.

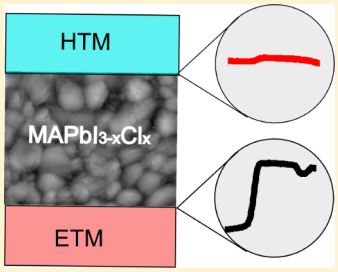

SECTION: Spectroscopy, Photochemistry, and Excited States

The metal organic halide perovskites are attractive candidates for absorber materials in a solar cell:[1] they have a sharp optical absorption edge and high absorption coefficients in the visible spectrum range, are chemically diverse (allowing tunability of the absorption edge),[2,3] are solution-processable, and form polycrystalline films composed of high-quality crystallites. This high quality leads to high electronic quality, with relatively low defect density, which contributes to their long charge-carrier diffusion lengths.[4−6] Solar cells, based on these interesting materials were reported with different configurations to give efficiencies, now approaching 18%.[7] Methylammonium lead iodide, synthesized with or without lead chloride as one of the starting materials ($MAPbI_{3-x}Cl_x$ or $MAPbI_3$, respectively), has been used to form highly efficient solar cells through various deposition techniques and device configurations.[8−10] Although quite efficient cells were made also without a hole-transporting material,[11−13] the most efficient cells to date were implemented with both electron-selective (e.g., TiO_2, ZnO, C60-derivatives) and hole-selective (e.g., doped spiro-MeOTAD, polytriarylamine) contacting materials. The role(s) of the hole-transporting material (HTM) and electron-transporting material (ETM) can be partially understood within the p-i-n model that was used to explain charge collection microscopic data of planar device cross sections.[14,15] Yet, the exact contributions of each selective contact to the photovoltaic action and, specifically to the open circuit voltage (V_{OC}), were not investigated directly.

Because, in general, these devices can show small ($E_{gap} - qV_{OC}$), it is of special interest and importance to try and identify the V_{OC} loss processes so as to further improve the device efficiencies.

Surface photovoltage (SPV) spectroscopy, measured using a macroscopic Kelvin probe setup, provides information on the role of the two charge-extracting interfaces that is complementary to the information gleaned from the dynamic approaches such as transient optical absorption[16] and time-resolved photoluminescence. A surface photovoltage is defined as the difference between the surface potential of a sample in the dark and under illumination. A nonzero SPV indicates redistribution of photogenerated free charges.[17] In samples of inorganic semiconductors with crystalline domains on a scale larger than a few to tens of nanometers, SPV most commonly results from photoinduced decrease in a built-in electrical potential gradient and flattening of the bands (canceling of the band bending) in a space-charge region, whether near the free surface of a semiconductor or around a buried interface.[18,19] The macroscopic Kelvin-probe method is contactless, non-destructive, and does not impose constraints such as transparent substrate. (See the Supporting Information for detailed description of the technique.) This allows measurement of the photovoltage of partial device structures and analysis of the contribution of each contact to the voltage. The SPV of a complete solar cell is of particular interest, as it closely corresponds to the open-circuit voltage under the same illumination conditions.[20,21]

Spectrally resolved SPV further extends the information that can be gleaned from these measurements and can provide detailed insight into the presence and effect of photoelectrically active intragap states. These could include interface states at the

Received: June 8, 2014
Accepted: June 23, 2014
Published: June 23, 2014

absorber/HTM or absorber/ETM heterointerfaces, surface states at the absorber grain boundaries, or bulk defect states. Following the response of the SPV spectrum to changes in the interfacing electrodes or changes in the fabrication process can help identify the origin of specific charge-separation processes.[22]

As part of our efforts to understand the mode of action of the perovskite-based solar cells, we report here results of our measurements of the SPV spectra of methylammonium lead iodide chloride ($MAPbI_{3-x}Cl_x$) perovskite absorber layers with several types of HTMs and ETMs.

Figure 1 shows the SPV spectrum of a (by now) conventional flat spiro-OMeTAD/$MAPbI_{3-x}Cl_x$/TiO_2/FTO

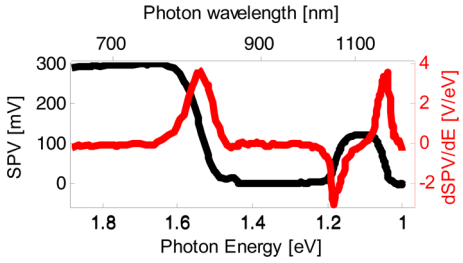

Figure 1. Surface photovoltage spectrum of spiro-OMeTAD/$MAPbI_{3-x}Cl_x$/TiO_2/FTO cell (black) and the derivative of the spectrum with respect to photon wavelength (red), showing the band-edge transition at ~1.5 eV and a composite IR feature at 1.0 to 1.2 eV.

cell,[14] illuminated from the spiro-OMeTAD side. The spectrum shows two prominent features, viz., the optical band edge at ~800 nm ("band-edge transition") and a shallow composite feature at 1050−1150 nm ("IR feature"). Because both features stem from light-induced redistribution of free charge carriers at high-intensity regions of the solar spectrum, they may be relevant to the cell's performance.

The band-edge transition is sharp, with a full width at half-maximum of the derivative of ~40 nm. This width is comparable to the transition widths measured on high-quality crystalline samples such as GaAs[23] and InP,[24] indicating a low density of gap states tailing from the band edges. This observation is in agreement with previous measurements on $MAPbI_3$ samples using other experimental methods.[25,26]

The complete cell of the type that we studied involves two selective contacts: TiO_2 on the electron-extracting side and spiro-OMeTAD on the hole-extracting side. Both interfaces may potentially induce band bending in the $MAPbI_{3-x}Cl_x$ and thus contribute to the SPV. The existence of band-bending was indeed reported at the $MAPbI_3$ on mesoporous TiO_2[27] interface but was excluded for the $MAPbI_{3-x}Cl_x$/spiro-OMeTAD interface.[28] However, band bending is determined by the Fermi-level alignment across the interface. Unlike what is the case for the spiro-OMeTAD that was deposited in situ for the XPS studies in ref 27, in the current study, the cells were kept in air overnight. This allows doping of the spiro-OMeTAD by oxygen from air, prior to measurement, as is done for fabricating efficient cells.[10,29] Such doping is expected to shift the Fermi level and hence the energy level alignment across the interface. We note in passing that the SPV can result from mechanisms other than band bending, as we discuss in the Supporting Information (SI).

The signals due to the electron drift toward the ETM and of the hole drift toward the HTM are summed up in the SPV regardless of the order of layer stacking, as depicted in Figure 2a,b. To isolate the independent contributions of each of the two junctions to the photovoltage, we compare the SPV spectrum before and after the deposition of an ETM or HTM on top of the $MAPbI_{3-x}Cl_x$. To decrease the sensitivity of the interpretation of the SPV measurements to possible cross-talk between the newly created top junction and the bottom junction,[30] we compare the case of ETM/$MAPbI_{3-x}Cl_x$/HTM to that of HTM/$MAPbI_{3-x}Cl_x$/ETM.

Figure 3 shows the SPV of an "inverted" stack of $MAPbI_{3-x}Cl_x$ on an HTM, poly(3,4-ethylenedioxythiophene) poly(styrenesulfonate) (PEDOT:PSS) (Figure 3a) or spiro-OMeTAD, (Figure 3b) before and after deposition of a top TiO_2 layer for electron extraction. We first consider the incomplete inverted cells, that is, those with a free $MAPbI_{3-x}Cl_x$

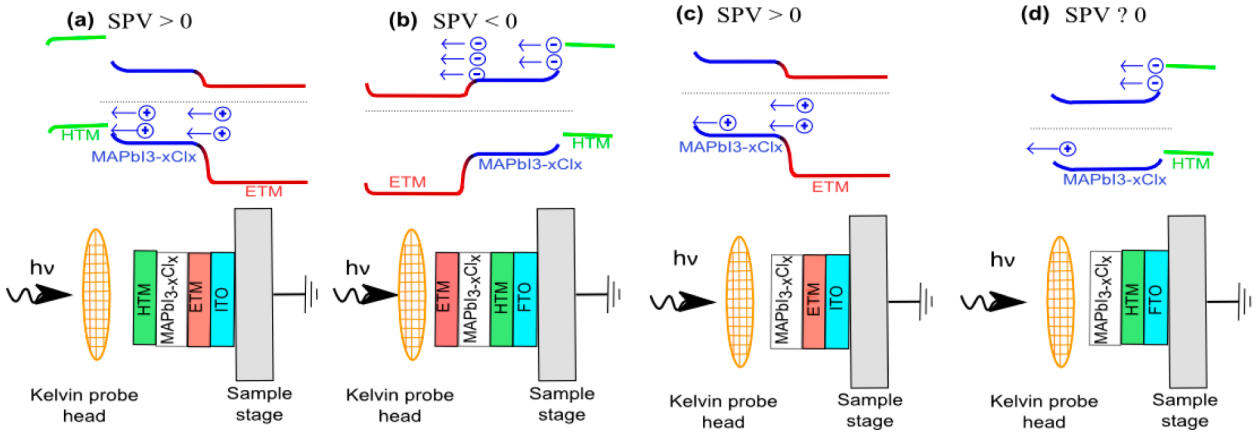

Figure 2. Band diagrams showing the charge accumulation at the side of the sample that was illuminated (the side facing the Kelvin probe): (a) Complete cell in "conventional" geometry. Holes diffuse to the surface from both the partially shaded absorber/ETM interface and the HTM/absorber interface to yield positive SPV. (b) Complete cell in "inverted" geometry; electrons diffuse to the surface from both the partially shaded absorber/HTM interface and ETM/absorber interface to yield negative SPV. (c) Incomplete cell in "conventional" geometry; holes diffuse to the surface from the partially shaded absorber/ETM interface and the space-charge region near the free surface to yield positive SPV. (d) Incomplete cell in "inverted" geometry; electrons diffuse from the absorber/HTM interface, and holes diffuse from the space-charge region near the free surface. The net SPV depends on the relative efficiency of charge separation at the surface versus that at the interface.

dx.doi.org/10.1021/jz501163r | J. Phys. Chem. Lett. 2014, 5, 2408−2413

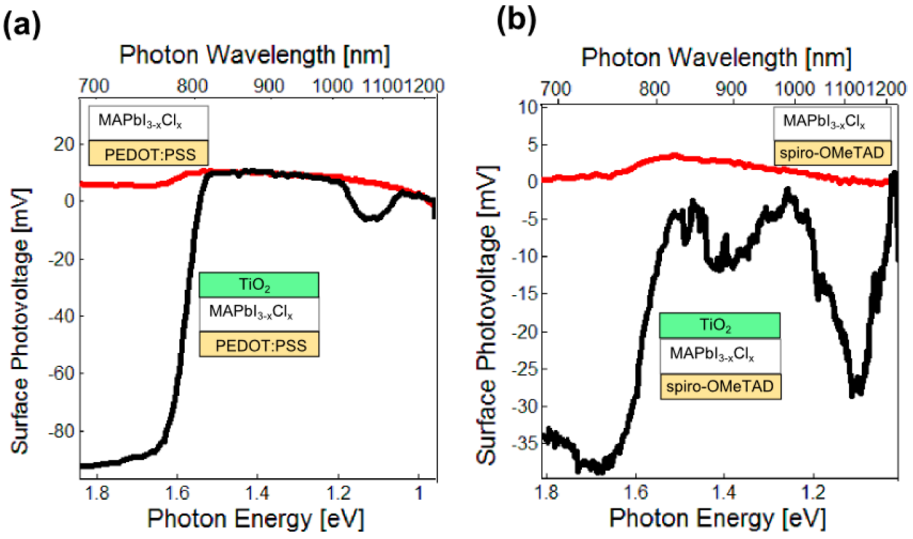

Figure 3. Surface photovoltage spectra of (a) $MAPbI_{3-x}Cl_x$/PEDOT:PSS/FTO and (b) $MAPbI_{3-x}Cl_x$/spiro-OMeTAD/FTO with (black) and without (red) a top layer of TiO_2. The photovoltage change across the band edge at 780 nm is 12 times stronger for the sample with TiO_2 layer compared with that of the sample with HTM layer only. The decrease in SPV at 1.1 eV is apparent only if the TiO_2 is present.

surface (cf. Figure 2d). A negative SPV develops at the band-edge transition with both HTM types, indicating that the surface potential has decreased by illuminating the stack. The free surface of an n-type semiconductor is expected to bend upward, and, upon supra-band gap illumination, generate a positive SPV signal, as the photogenerated free electrons reduce the depletion. Previously we observed such upward band bending at the grain boundaries of $MAPbI_3$ using scanning Kelvin probe microscopy.[15] Therefore, the negative sign of the SPV of the incomplete inverted cells indicates a higher efficiency of charge separation at the buried HTM interface than at the free surface. The canceling out of free charges originating from the HTM/$MAPbI_{3-x}Cl_x$ interface and from the $MAPbI_{3-x}Cl_x$ surface reduces the amplitude of the absorption edge transition of the incomplete inverted cell to a few millivolts. The IR feature around 1100 nm is further reduced to below the instrumental sensitivity of ∼1 mV. When a TiO_2 layer is deposited on top of the $MAPbI_{3-x}Cl_x$ (cf. Figure 2b), the SPV at the band edge transition increases by an order of magnitude, and the IR feature is restored. This indicates that the ETM/$MAPbI_{3-x}Cl_x$ interface is the dominant one for photovoltage generation and therefore is the dominant contributor to the complete cell voltage under operation conditions.

In addition, Figure 4 shows the SPV of $MAPbI_{3-x}Cl_x$ on TiO_2 ("conventional" configuration), where deposition of p-doped spiro-OMeTAD as top HTM contributes up to 30% of the overall photovoltage at the band-edge transition. The dominance in charge separation of the TiO_2/$MAPbI_{3-x}Cl_x$ over the $MAPbI_{3-x}Cl_x$/spiro-OMeTAD interface is clear, especially considering that <30% of the supra-bandgap photons reach the back TiO_2 interface. (See Figure S2a in the SI for the $MAPbI_{3-x}Cl_x$ transmittance spectrum.) Consequently, the initial population of excited electrons in the immediate vicinity of the interface with TiO_2 is smaller than that near the interface with spiro-OMeTAD. The dominance of the TiO_2 interface was also observed by transient absorption spectroscopy,[31] where 70% of the charge-separation signal was attributed to electron injection into TiO_2. Furthermore, our observation agrees with the higher charge-extracting efficiency at the ETM than at the

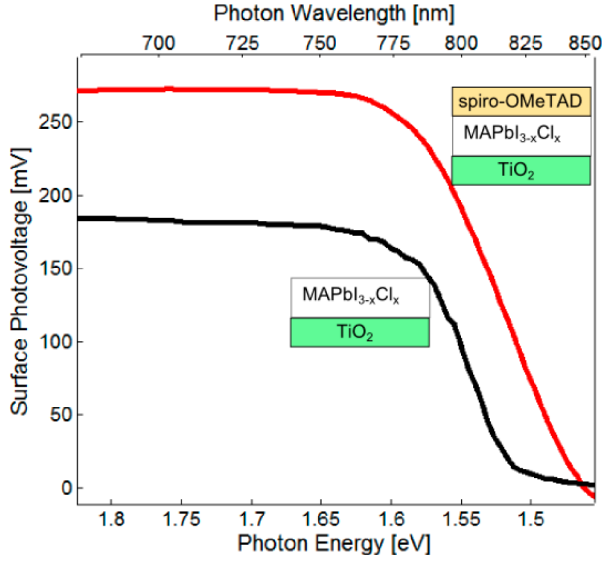

Figure 4. Surface photovoltage spectra of $MAPbI_{3-x}Cl_x$/TiO_2/ITO with (red) and without (black) a top layer of spiro-OMeTAD. The addition of the HTM contributes ∼30% of the overall photovoltage above the band gap.

HTM interface, as was previously found to be the case in scanning electron beam-induced current experiments.[14] The red shift of the band-edge transition that follows the deposition of the HTM (cf. Figure 4) can be explained by field-assisted photoexcitation at the HTM/$MAPbI_{3-x}Cl_x$ interface, known as the Franz−Keldysh effect.[32] The shift of the SPV cutoff indicates the existence of stronger internal field at the spiro-OMeTAD/$MAPbI_{3-x}Cl_x$ interface than at the free surface of the $MAPbI_{3-x}Cl_x$, prior to HTM deposition. (See the SI for further discussion.) We note that a red shift may also occur due to the creation of shallow trap states upon top-layer deposition. However, if that were the case then we would expect a broadening of the transition, which is not observed. Photovoltaic efficiency surveys of $CH_3NH_3PbI_3$-based devices with various HTM[33−35] materials showed an increase of 20−40% in open-circuit voltage upon the introduction of an HTM.

dx.doi.org/10.1021/jz501163r | J. Phys. Chem. Lett. 2014, 5, 2408−2413

The observation of relative contributions of ETM and HTM interfaces is not unique to TiO_2; C60 and its derivatives were reported as alternative ETMs in an efficient perovskite-based solar cell.[36,37]

In Figure 5, C60 is used as ETM rather than TiO_2. The addition of C60 increases the SPV signal magnitude at the

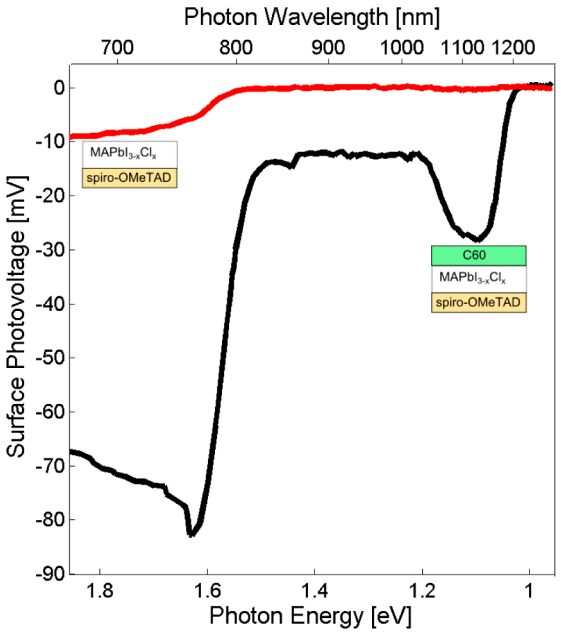

Figure 5. Surface photovoltage spectra of $MAPbI_{3-x}Cl_x$/PEDOT:PSS/FTO with (black) and without (red) a top layer of C60.

absorption edge by an order of magnitude (from <1 mV to >16 mV). Furthermore, the IR spectral feature that previously appeared only when TiO_2 is in contact with $MAPbI_{3-x}Cl_x$, is observed with C60 as ETM as well. A similar broad feature at 1000−1400 nm was also observed in photoinduced absorption spectroscopy of the $MAPbI_3/TiO_2$ interface and was attributed to an electron-transfer process from the perovskite to the TiO_2.[38]Figure 6 shows, however, that this feature is not specific for TiO_2 and is also observed in junctions of $MAPbI_{3-x}Cl_x$ with SnO_2 and C60.

The presence of the ETM enhances the IR feature not only in the SPV spectrum but also in the optical transmittance spectrum (Figure S2b in the SI), possibly due to field-assisted absorption. The spectral position of the 1100 nm feature is invariant under change of ETM type. Moreover, the IR features appear at the same position also if $MAPbI_3$ is used as absorber instead and appears to be insensitive to process parameters, such as the solvents used and the initial inclusion of Cl or HI additives. (See the SI for further details.) However, the magnitude of the feature depends on the absorber morphology (Figures S5 and S6 in the SI). We speculate that the feature is related to a reduced effective band gap at the grain boundaries, as suggested by the IR response of the grain boundaries when scanned with Kelvin-probe microscope (Figure S8 in the SI). Better understanding of the source of this feature and its relation to the performance of a working cell requires further investigation.

To summarize, we have studied the contributions of the electron- and hole-transport materials to the photovoltage of a solar cell based on a $MAPbI_{3-x}Cl_x$ perovskite absorber. Using the Kelvin-probe technique, we show directly that the electron-

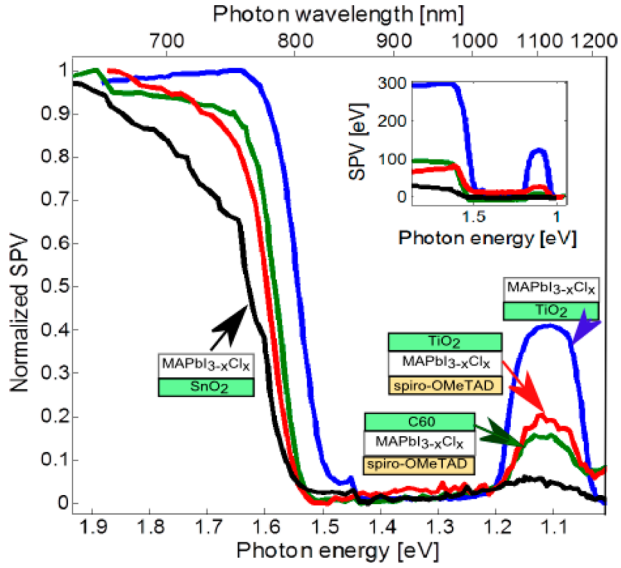

Figure 6. Surface photovoltage spectra of $MAPbI_{3-x}Cl_x$ with various electron-transport layers: TiO_2 as top (red) or bottom (blue) electrode, C60 (green), and SnO_2(black). The IR feature has the same spectral position for all layers. Inset: absolute SPV spectra. The shift of SPV onset at the band edge is possibly due to Franz−Keldysh effect or to morphological changes within the $MAPbI_{3-x}Cl_x$ film.

selective junction contributes most of the solar-illumination-induced photovoltage. We therefore confirm that the electron-selective junction is dominant in determining the open-circuit voltage. Furthermore, we show that this junction is related to a spectral feature at 1.1 eV, the origin and photovoltaic importance of which remains to be determined. Our results illustrate the usefulness of the relatively simple SPV spectroscopy in enhancing understanding of charge injection processes in perovskite-based photovoltaics.

EXPERIMENTAL METHODS

Sample Fabrication. The preparation of fluorine-doped tin oxide (FTO) and compact TiO_2 substrate as well as preparation and deposition of $MAPbI_{3-x}Cl_x$ were described elsewhere.[28] The film thickness was not uniform and varied in the range of 400−900 nm.

TiO_2 as a top layer (i.e., deposited onto $MAPbI_{3-x}Cl_x$) was spin-coated from a sol−gel solution prepared according to a published literature procedure.[39] In short, titanium isopropoxide was mixed with a dilute HCl solution in isopropanol to yield a 0.026 M concentration solution. The solution was filtered with a PTFE filter with 0.22 μm pore size before use. The resulting TiO_2 thickness was 40−50 nm.

A film of hole conductor was deposited onto $MAPbI_{3-x}Cl_x$ by spin-coating at 2000 rpm for 45 s an 80 mg/mL Spiro-MeOTAD solution in chlorobenzene to which 7 μL of *tert*-butylpyridine and 15 μL of LiTFSI solution (170 mg/mL in acetonitrile) were added. The resulting film thickness was 200−500 nm, depending on the thickness of the underlying $MAPbI_{3-x}Cl_x$. A 30 nm top layer of C60 was deposited onto the $MAPbI_{3-x}Cl_x$ layer by thermal evaporation.

For the inverted cell configuration, glass coated with indium tin oxide (ITO) was used as substrate. It was cleaned by solvent sonication before spin-coating of the HTM layer. Spiro-MeOTAD was applied as previously described and left overnight in the dark in dry air (relative humidity <20%) to

dx.doi.org/10.1021/jz501163r | J. Phys. Chem. Lett. 2014, 5, 2408−2413

allow (p-)doping by oxygen from air. A film of 100 nm of PEDOT:PSS (Clevios PH-1000, Heraeus), doped with 5% ethylene glycol and 0.4% zonyl surfactant, was deposited by spin-coating and annealed for 30 min at 150 °C in a dry N_2 environment.

SPV Measurements. The contact potential difference (CPD) between the sample and a gold grid reference electrode was measured in a Kelvin-probe configuration using a Besocke Delta-Phi probe and controller. The sample was illuminated from a 600 W tungsten−halogen lamp with wavelength selection by 1/4 m monochromator. The wavelength resolution was 0.6 nm. The SPV was defined as {CPD(dark) − CPD(light)}. The samples were allowed to stabilize in the dark for 3 h prior to measurement. The dwelling time on each wavelength was a few minutes, until the signal stabilized (i.e., changed <0.3 mV over the time span of 1 min). The scan direction was from long to short wavelength to minimize possible effects of radiative recombination from long-lived trap states. To avoid degradation of the perovskite layer, we conducted the measurement in a dry N_2 environment in a glovebox.

■ ASSOCIATED CONTENT

Supporting Information

Overview of the Kelvin probe technique; transmittance spectra; discussion on possible sources of SPV signal other than band bending; discussion of the source of red-shift of the band edge; discussion of the relations between morphology and IR feature. This material is available free of charge via the Internet at http://pubs.acs.org.

■ AUTHOR INFORMATION

Corresponding Authors

*E-mail: gary.hodes@weizmann.ac.il.
*E-mail: david.cahen@weizmann.ac.il.

Notes

The authors declare no competing financial interest.

■ ACKNOWLEDGMENTS

We thank Leeor Kronik (WIS) for illuminating discussions, Sabyasachi Mukhopadhyay (WIS) for conducting scanning Kelvin probe measurements, Arie Zaban (Bar-Ilan Univ., Israel) for providing the SnO_2 samples, and the Leona M. and Harry B. Helmsley Charitable Trust, the Israel Ministry of Science's "Tashtiot" program, the Israel National Nano-Initiative's Focused Technology Area program, the Nancy and Stephen Grand Center for Sensors and Security, and the Weizmann-U.K. Joint Research Program for support. D.C. holds the Sylvia and Rowland Schaefer Chair in Energy Research.

■ REFERENCES

(1) Snaith, H. J. Perovskites: The Emergence of a New Era for Low-Cost, High-Efficiency Solar Cells. *J. Phys. Chem. Lett.* **2013**, *4*, 3623−3630.

(2) Noh, J. H.; Im, S. H.; Heo, J. H.; Mandal, T. N.; Seok, S. I. Chemical Management for Colorful, Efficient, and Stable Inorganic−Organic Hybrid Nanostructured Solar Cells. *Nano Lett.* **2013**, *13*, 1764−1769.

(3) Eperon, G. E.; Stranks, S. D.; Menelaou, C.; Johnston, M. B.; Herz, L. M.; Snaith, H. J. Formamidinium Lead Trihalide: A Broadly Tunable Perovskite for Efficient Planar Heterojunction Solar Cells. *Energy Environ. Sci.* **2014**, *7*, 982−988.

(4) Stranks, S. D.; Eperon, G. E.; Grancini, G.; Menelaou, C.; Alcocer, M. J. P.; Leijtens, T.; Herz, L. M.; Petrozza, A.; Snaith, H. J. Electron-Hole Diffusion Lengths Exceeding 1 Micrometer in an Organometal Trihalide Perovskite Absorber. *Science* **2013**, *342*, 341−344.

(5) Wehrenfennig, C.; Eperon, G. E.; Johnston, M. B.; Snaith, H. J.; Herz, L. M. High Charge Carrier Mobilities and Lifetimes in Organolead Trihalide Perovskites. *Adv. Mater.* **2014**, *26*, 1584−1589.

(6) Xing, G.; Mathews, N.; Sun, S.; Lim, S. S.; Lam, Y. M.; Gratzel, M.; Mhaisalkar, S.; Sum, T. C. Long-Range Balanced Electron- and Hole-Transport Lengths in Organic-Inorganic $CH_3NH_3PbI_3$. *Science* **2013**, *342*, 344−347.

(7) National Center for Photovoltaics. *NREL Best Research-Cell Efficiencies Chart*; National Renewable Energy Laboratory: Boulder, CO, 2014.

(8) Liu, D.; Kelly, T. L. Perovskite Solar Cells with a Planar Heterojunction Structure Prepared Using Room-Temperature Solution Processing Techniques. *Nat. Photonics* **2013**, *8*, 133−138.

(9) Burschka, J.; Pellet, N.; Moon, S.-J.; Humphry-Baker, R.; Gao, P.; Nazeeruddin, M. K.; Grätzel, M. Sequential Deposition as a Route to High-Performance Perovskite-Sensitized Solar Cells. *Nature* **2013**, *499*, 316−319.

(10) Liu, M.; Johnston, M. B.; Snaith, H. J. Efficient Planar Heterojunction Perovskite Solar Cells by Vapour Deposition. *Nature* **2013**, *501*, 395−398.

(11) Etgar, L.; Gao, P.; Xue, Z.; Peng, Q.; Chandiran, A. K.; Liu, B.; Nazeeruddin, M. K.; Grätzel, M. Mesoscopic $CH_3NH_3PbI_3/TiO_2$ Heterojunction Solar Cells. *J. Am. Chem. Soc.* **2012**, *134*, 17396−17399.

(12) Aharon, S.; Gamliel, S.; Cohen, B. E.; Etgar, L. Depletion Region Effect of Highly Efficient Hole Conductor Free $CH_3NH_3PbI_3$ Perovskite Solar Cells. *Phys. Chem. Chem. Phys.* **2014**, *16*, 10512−10518.

(13) Shi, J.; Luo, Y.; Wei, H.; Luo, J.; Dong, J.; Lv, S.; Xiao, J.; Xu, Y.; Zhu, L.; Xu, X.; Wu, H.; Li, D.; Meng, Q. Modified Two-Step Deposition Method for High-Efficiency $TiO_2/CH_3NH_3PbI_3$ Heterojunction Solar Cells. *ACS Appl. Mater. Interfaces* **2014**, DOI: 10.1021/am502131t.

(14) Edri, E.; Kirmayer, S.; Mukhopadhyay, S.; Gartsman, K.; Hodes, G.; Cahen, D. Elucidating the Charge Carrier Separation and Working Mechanism of $CH_3NH_3PbI_{3-x}Cl_x$ Perovskite Solar Cells. *Nat. Commun.* **2014**, *5*, 3461.

(15) Edri, E.; Kirmayer, S.; Henning, A.; Mukhopadhyay, S.; Gartsman, K.; Rosenwaks, Y.; Hodes, G.; Cahen, D. Why Lead Methylammonium Tri-Iodide Perovskite-Based Solar Cells Require a Mesoporous Electron Transporting Scaffold (but Not Necessarily a Hole Conductor). *Nano Lett.* **2014**, *14*, 1000−1004.

(16) Kim, H.-S.; Lee, C.-R.; Im, J.-H.; Lee, K.-B.; Moehl, T.; Marchioro, A.; Moon, S.-J.; Humphry-Baker, R.; Yum, J.-H.; Moser, J. E.; Grätzel, M.; Park, N.-G. Lead Iodide Perovskite Sensitized All-Solid-State Submicron Thin Film Mesoscopic Solar Cell with Efficiency Exceeding 9%. *Sci. Rep.* **2012**, *2*, 591.

(17) Kronik, L.; Shapira, Y. Surface Photovoltage Phenomena: Theory, Experiment, and Applications. *Surf. Sci. Rep.* **1999**, *37*, 1−206.

(18) Gal, D.; Beier, J.; Moons, E.; Hodes, G.; Cahen, D.; Kronik, L.; Burstein, L.; Mishori, B.; Leibovitch, M.; Shapira, Y. Band Diagram and Band Line-up of the Polycrystalline CdS/Cu(In,Ga)Se2 Heterojunction and Its Response to Air Annealing. *AIP Conf. Proc.* **1996**, *353*, 453−464.

(19) Gross, D.; Mora-Seró, I.; Dittrich, T.; Belaidi, A.; Mauser, C.; Houtepen, A. J.; Como, E. D.; Rogach, A. L.; Feldmann, J. Charge Separation in Type II Tunneling Multilayered Structures of CdTe and CdSe Nanocrystals Directly Proven by Surface Photovoltage Spectroscopy. *J. Am. Chem. Soc.* **2010**, *132*, 5981−5983.

(20) Kronenberg, N. M.; Deppisch, M.; Würthner, F.; Lademann, H. W. A.; Deing, K.; Meerholz, K. Bulk Heterojunction Organic Solar Cells Based on Merocyanine Colorants. *Chem. Commun.* **2008**, 6489.

(21) Lee, Y.-J.; Wang, J.; Hsu, J. W. P. Surface Photovoltage Characterization of Organic Photovoltaic Devices. *Appl. Phys. Lett.* **2013**, *103*, 173302.
(22) Osterloh, F. E.; Holmes, M. A.; Chang, L.; Moulé, A. J.; Zhao, J. Photochemical Charge Separation in Poly(3-Hexylthiophene) (P3HT) Films Observed with Surface Photovoltage Spectroscopy. *J. Phys. Chem. C* **2013**, *117*, 26905−26913.
(23) Burstein, L.; Bregman, J.; Shapira, Y. Surface Photovoltage Spectroscopy of Gap States at GaAs and InP Metal Interfaces. *Appl. Phys. Lett.* **1990**, *57*, 2466−2468.
(24) Bastide, S.; Gal, D.; Cahen, D.; Kronik, L. Surface Photovoltage Measurements in Liquids. *Rev. Sci. Instrum.* **1999**, *70*, 4032−4036.
(25) De Wolf, S.; Holovsky, J.; Moon, S.-J.; Löper, P.; Niesen, B.; Ledinsky, M.; Haug, F.-J.; Yum, J.-H.; Ballif, C. Organometallic Halide Perovskites: Sharp Optical Absorption Edge and Its Relation to Photovoltaic Performance. *J. Phys. Chem. Lett.* **2014**, *5*, 1035−1039.
(26) Yamada, Y.; Nakamura, T.; Endo, M.; Wakamiya, A.; Kanemitsu, Y. Near-Band-Edge Optical Responses of Solution-Processed Organic−inorganic Hybrid Perovskite $CH_3NH_3PbI_3$ on Mesoporous TiO_2 Electrodes. *Appl. Phys. Express* **2014**, *7*, 032302.
(27) Laban, W. A.; Etgar, L. Depleted Hole Conductor-Free Lead Halide Iodide Heterojunction Solar Cells. *Energy Environ. Sci.* **2013**, *6*, 3249−3253.
(28) Schulz, P.; Edri, E.; Kirmayer, S.; Hodes, G.; Cahen, D.; Kahn, A. Interface Energetics in Organo-Metal Halide Perovskite-Based Photovoltaic Cells. *Energy Environ. Sci.* **2014**, *7*, 1377−1381.
(29) Lee, M. M.; Teuscher, J.; Miyasaka, T.; Murakami, T. N.; Snaith, H. J. Efficient Hybrid Solar Cells Based on Meso-Superstructured Organometal Halide Perovskites. *Science* **2012**, *338*, 643−647.
(30) Itzhaik, Y.; Hodes, G.; Cohen, H. Band Alignment and Internal Field Mapping in Solar Cells. *J. Phys. Chem. Lett.* **2011**, *2*, 2872−2876.
(31) Marchioro, A.; Teuscher, J.; Friedrich, D.; Kunst, M.; van de Krol, R.; Moehl, T.; Grätzel, M.; Moser, J.-E. Unravelling the Mechanism of Photoinduced Charge Transfer Processes in Lead Iodide Perovskite Solar Cells. *Nat. Photonics* **2014**, *8*, 250−255.
(32) Seeger, K. *Semiconductor Physics: An Introduction*; Springer: Berlin, 1999.
(33) Heo, J. H.; Im, S. H.; Noh, J. H.; Mandal, T. N.; Lim, C.-S.; Chang, J. A.; Lee, Y. H.; Kim, H.; Sarkar, A.; Nazeeruddin, M. K.; et al. Efficient Inorganic-Organic Hybrid Heterojunction Solar Cells Containing Perovskite Compound and Polymeric Hole Conductors. *Nat. Photonics* **2013**, *7*, 486−491.
(34) Jeon, N. J.; Lee, J.; Noh, J. H.; Nazeeruddin, M. K.; Grätzel, M.; Seok, S. I. Efficient Inorganic−Organic Hybrid Perovskite Solar Cells Based on Pyrene Arylamine Derivatives as Hole-Transporting Materials. *J. Am. Chem. Soc.* **2013**, *135*, 19087−19090.
(35) Juarez-Perez, E. J.; Wuβler, M.; Fabregat-Santiago, F.; Lakus-Wollny, K.; Mankel, E.; Mayer, T.; Jaegermann, W.; Mora-Sero, I. Role of the Selective Contacts in the Performance of Lead Halide Perovskite Solar Cells. *J. Phys. Chem. Lett.* **2014**, *5*, 680−685.
(36) Malinkiewicz, O.; Yella, A.; Lee, Y. H.; Espallargas, G. M.; Graetzel, M.; Nazeeruddin, M. K.; Bolink, H. J. Perovskite Solar Cells Employing Organic Charge-Transport Layers. *Nat. Photonics* **2014**, *8*, 128−132.
(37) You, J.; Hong, Z.; Yang, Y.; Chen, Q.; Cai, M.; Song, T.-B.; Chen, C.-C.; Lu, S.; Liu, Y.; Zhou, H.; Yang, Y. Low-Temperature Solution-Processed Perovskite Solar Cells with High Efficiency and Flexibility. *ACS Nano* **2014**, *8*, 1674−1680.
(38) Bi, D.; Yang, L.; Boschloo, G.; Hagfeldt, A.; Johansson, E. M. J. Effect of Different Hole Transport Materials on Recombination in $CH_3NH_3PbI_3$ Perovskite-Sensitized Mesoscopic Solar Cells. *J. Phys. Chem. Lett.* **2013**, *4*, 1532−1536.
(39) Docampo, P.; Ball, J. M.; Darwich, M.; Eperon, G. E.; Snaith, H. J. Efficient Organometal Trihalide Perovskite Planar-Heterojunction Solar Cells on Flexible Polymer Substrates. *Nat. Commun.* **2013**, *4*, 2761.